Coupled Systems Mechanics, *Vol. 14, No. 6 (2025) 575-594*
https://doi.org/10.12989/csm.2025.14.6.575

Guided wave propagation in porous functionally graded doubly curved nano-shells with different boundary conditions

Kuineng Chen[1], Zipan Yang[2] and Wubin Shan*[3]

[1]*Hunan Vocational Institute of Technology, Xiangtan 411104, China*
[2]*Xiangtan Hengxin Industrial Co., Ltd., Xiangtan, 411300, China*
[3]*College of Mechanical and Vehicle Engineering, Hunan University, Changsha, 410082, China*

(Received November 5, 2025, Revised January 2, 2026, Accepted January 20, 2026)

Abstract. Despite significant interest in the mechanics of nanostructures, the propagation behavior of guided waves in porous functionally graded (FG) doubly-curved nanoshells remains unexplored, particularly concerning the influence of different boundary constraints. The present study is therefore dedicated to addressing this void by developing a comprehensive analytical model for this problem. Based on the nonlocal strain gradient theory (NSGT) framework and incorporating the effect of moment of inertia, the governing equations of motion for porous functionally graded doubly curved shells are derived. The Galerkin technique is employed to eliminate the spatial variables from the partial differential equation system, thereby converting it into an ordinary differential equation with respect to time. By applying the boundary conditions and solving the characteristic equation, the dispersion characteristics of porous functionally graded strain gradient doubly curved shells with different boundary conditions are determined. The results indicate that the phase velocity of the hyperbolic curved plate is the smallest, followed by the cylindrical curved plate, then the ellipsoidal curved plate, with the spherical shell exhibiting the maximum phase velocity. Clearly, the spherical shell has the highest stiffness, naturally resulting in the maximum phase velocity. Additionally, at low wave numbers, the effects of nonlocal and strain gradient parameters on the dispersion relation are negligible.

Keywords: functionally graded porous material; guided wave; nanoshells; nonlocal strain gradient theory

1. Introduction

Nano-shells, as a class of nanomaterials with unique structural properties, are of critical importance in understanding the physicochemical behavior at the nanoscale (Faleh *et al.* 2018). By thoroughly investigating the dynamic characteristics of nano-shells, such as surface atomic migration, interfacial interactions, and rapid response mechanisms to external stimuli, we can uncover their potential applications in fields like catalysis, sensing, and biomedicine. For instance, in catalytic processes (Lata and Kaur 2024), the dynamic behavior of nano-shells directly influences reaction rates and selectivity, while in biomedicine, their kinetic properties determine the precision of drug delivery and biocompatibility. Therefore, studying the dynamic behavior of

*Corresponding author, Ph.D., E-mail: shanwubin2020@163.com

 ISSN: 2234-2184 (Print), 2234-2192 (Online)

nano-shells not only aids in optimizing material design but also drives innovative applications of nanotechnology in key areas such as energy, the environment, and healthcare, providing crucial support for future technological advancements (Karami *et al.* 2018). Recent studies have explored the dynamic and vibrational characteristics of various nanostructures. Li *et al.* (2025) investigated the free vibration of FG spherical shallow nanoshells, incorporating porosity effects and employing Eringen's nonlocal elasticity theory to account for small-scale phenomena. Van *et al.* (2025) proposed a meshfree method to analyze the natural and forced vibrations of a tri-directionally FG porous doubly-curved nanoshell with magneto-electro-elastic layers on a viscoelastic foundation, featuring a porous core and surface layers. Mirfatah *et al.* (2025) studied the nonlinear forced vibration of doubly curved sandwich nano-shells resting on a Winkler-Pasternak foundation, using the Galerkin method. Thuy *et al.* (2025) examined the random vibration of biaxially curved nanoshells with piezoelectric layers on viscoelastic foundations. Jiammeepreecha *et al.* (2025) developed an effective nonlocal finite element method to assess the free vibration of sigmoid FG material nanoshells. Mansouri *et al.* (2024) investigated the nonlinear forced vibration of truncated open conical nanoshells, incorporating nonlocal elasticity and von Kármán nonlinear strains. Vinh *et al.* (2023) analyzed the free vibration of FG porous doubly curved shallow nanoshells with variable nonlocal parameters, modifying Eringen's theory. Khorshidi *et al.* (2022) studied the vibration of FG conical nanoshells with piezoelectric and flexoelectric effects, featuring a sandwich structure. Vinh and Tounsi (2022) applied a nonlocal first-order shear deformation theory with variable parameters to assess the free vibration of FG doubly curved nanoshells using Navier' solution.

However, research on wave propagation characteristics in nanoshells structures remains relatively scarce. Current academic exploration into key issues such as the propagation laws, attenuation mechanisms, and energy dissipation of mechanical, electromagnetic, or acoustic waves in shell-shaped nanostructures is still in its infancy, with particularly scarce systematic studies. This research gap not only limits the application potential of nanoshells structures in fields like sensors, energy harvesting, and biomedicine but also hinders a deeper understanding of the wave-structure interaction mechanisms at the nanoscale. Recent studies have explored wave propagation in various nanoshell configurations, employing different theoretical frameworks. Ebrahimi *et al.* (2024) investigated the impact of temporal nonlocality on wave dynamics in viscoelastic FGM nanoshells, deriving governing equations and obtaining analytical solutions for wave frequency and phase velocity. Wang *et al.* (2023a) studied wave characteristics in bidirectionally graded porous nanoshells using nonlocal equations derived from Hamilton's principle. In a related study, Wang *et al.* (2023b) examined wave behavior in porous FGPM nanoshells on viscoelastic foundations, highlighting the significant influence of porosity and Pasternak parameters at small thicknesses. Ebrahimi *et al.* (2022) demonstrated that viscoelastic behavior in nanoscale waveguides requires more sophisticated nonlocal theories when wavelengths approach the nanostructure's characteristic length. Ardalani *et al.* (2022) analyzed fluid-conveying flexoelectric cylindrical nanoshells under electric fields, developing a new model combining NSGT with flexoelectric relations. Yang *et al.* (2019) investigated FG cylindrical nanoshells using nonlocal Flugge shell theory, with parametric studies on power-law exponent, wave number, nonlocal parameter, and radius-to-thickness ratio. Karami *et al.* (2019) focused on porous nanoshells using Bi-Helmholtz nonlocal strain gradient theory with higher-order shear deformation theory. Ma *et al.* (2018) studied MEE nanoshells via Kirchhoff-Love and first-order shear deformation theories. Zeighampour *et al.* (2017) examined wave propagation in laminated cylindrical nanoshells, considering combined nonlocal and strain gradient effects using thin shell theory. These studies

collectively advance the understanding of wave-structure interactions at the nanoscale. In addition, Atmane and collaborators (Benadouda *et al*. 2025, Bennai *et al*. 2022a, 2022b, 2022c, Bourouis *et al.* 2025, Dahmane *et al.* 2024a, 2024b, 2024c, Djebbour *et al*. 2024, Ghalem *et al*. 2025, Khayra *et al.* 2024, Mellal *et al*. 2021, 2023, Nebab *et al.* 2024a, 2024b, 2024c) focused on the dynamic response and wave propagation characteristics of functional graded material structures. They systematically investigate the effects of defects such as porosity and cracks on wave propagation, vibration, and stability, and commonly employ advanced mechanical models for analysis. More relevant works can refer to (Hu and Li 2018, 2019, Hu and Wang 2015, 2016, Hu *et al.* 2018, Hu and Ma 2019, Hu and Xu 2021, Li and Hu 2021, Li *et al.* 2024, 2017, She and He 2025, Cheng and She 2025a, 2025b, Cheng *et al.* 2025, Fan and She 2025, 2026, Fan *et al.* 2025)

However, there is no paper analyzing the guided wave propagation in porous functionally graded doubly curved nano-shells with different boundary conditions, the present paper aims to solve this problem. Based on the NSGT framework and accounting for the moment of inertia, the governing equations of motion for porous functionally graded doubly curved shells are derived. The Galerkin technique (Ma *et al*. 2026, Zhao and She 2025, Zhao *et al.* 2025, She *et al*. 2026) is applied to eliminate the spatial variables from the system of partial differential equations, reducing it to an ordinary differential equation in terms of time. By incorporating boundary conditions and solving the characteristic equation, the dispersion characteristics of porous functionally graded strain gradient doubly curved shells under different boundary conditions are analyzed. The results demonstrate that the phase velocity is lowest in the hyperbolic curved plate, followed by the cylindrical curved plate, then the ellipsoidal curved plate, with the spherical shell exhibiting the highest phase velocity. This is expected, as the spherical shell possesses the greatest stiffness, leading to the maximum phase velocity. Furthermore, at low wave numbers, the influence of nonlocal and strain gradient parameters on the dispersion relation is negligible. However, at high wave numbers, these parameters significantly affect both phase and group velocities. Specifically, the nonlocal parameter induces a stiffness-softening effect, whereas the strain gradient parameter produces a stiffness-strengthening effect.

2. Theoretical modeling

The FG doubly curved nanoshells under consideration, as depicted in Fig. 1, are composed of a combination of ceramic and metal materials. The nomenclature used in this paper is provided in Table 1. The equivalent elastic modulus $E_f(z)$, Poisson's ratio $v_f(z)$, and mass density $\rho_f(z)$ can be expressed as functions of the power law index (N) and the volume fraction of porosity (p) (Faleh *et al*. 2018).

$$E_f(z) = E_m + \left(\frac{z}{h} + \frac{1}{2}\right)^N (E_c - E_m) - \frac{p}{2}(E_c + E_m) \tag{1a}$$

$$v_f(z) = v_m + \left(\frac{z}{h} + \frac{1}{2}\right)^N (v_c - v_m) - \frac{p}{2}(v_c + v_m) \tag{1b}$$

$$\rho_f(z) = \rho_m + \left(\frac{z}{h} + \frac{1}{2}\right)^N (\rho_c - \rho_m) - \frac{p}{2}(\rho_c + \rho_m) \tag{1c}$$

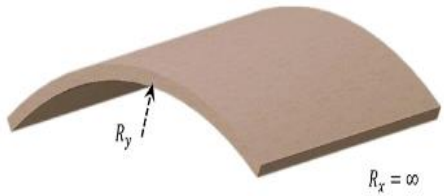

(a) Cylindrical shell ($R_x \rightarrow \infty$, $R_y=a$)

(b) Spherical shell ($R_x=R_y=a$)

(c) Ellipsoidal shell ($R_x=a$, $R_y=2a$)

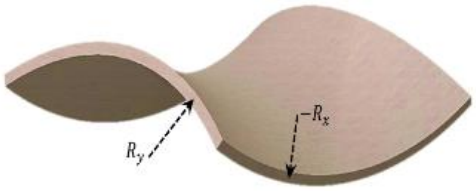

(d) Hyperbolic shell ($R_x=a$, $R_y=-a$)

Fig. 1 The sketch of doubly curved shells (Modified from Khaniki and Ghayesh 2023, Badarloo *et al.* 2022)

Table 1 Nomenclature

Nomenclature	
R_x and R_y	transverse and longitudinal curvature radii of the nanoshell
h	the thickness of the nanoshell
$E_f(z), v_f(z), \rho_f(z)$	the equivalent elastic modulus, Poisson's ratio, and mass density of the nanoshell
N	power law index
p	the volume fraction of porosity
E_c, E_m	the elastic modulus of ceramic and metal phases
v_c, v_m	the Poisson's ratio of ceramic and metal phases
ρ_c, ρ_m	the mass density of ceramic and metal phases
$u(x,y,z,t), v(x,y,z,t), w(x,y,z,t)$	the displacements components of points lying on the nanoshell domain
t	time
$u_0(x,y,t), v_0(x,y,t), w_0(x,y,t)$	the displacements of a generic point on the middle surface for the doubly nanoshell
$\varphi_x(x,y,t), \varphi_y(x,y,t)$	the in-plane rotational displacements of the cross-section
ε_{xx}, ε_{yy} and γ_{xy}	membrane strains
γ_{xz} and γ_{yz}	the transverse strains
$\sigma_{xx}, \sigma_{yy}, \sigma_{xz}, \sigma_{yz}, \sigma_{xy}$	the normal stress and shear stress
$Q_{11}, Q_{12}, Q_{12}, Q_{22}, Q_{44}, Q_{55}, Q_{66}$	the equivalent stiffness coefficient
∇^2	Laplace operator
$N_x, N_y, N_{xy}, M_x, M_y, M_{xy}, T_x, T_y, T_{xy}$	internal forces and moment
$T_x, T_y, T_{xy}, Q_x, Q_y, S_x, S_y$	shear force and shear moment
$I_1, I_2, I_3, I_4, I_5, I_7$	moment of inertia and generalized moment of inertia
u_{mn},v_{mn},w_{mn},ϕ_{mn}^x and ϕ_{mn}^y	wave amplitudes
k_1 and k_2	the wave numbers along the x- and y-directions
ω	the circular frequency
C_p	phase velocity
C_g	group velocity
K	stiffness Coefficient matrix
M	mass coefficient matrix

In the given Eq. (1), the subscripts *m* and *c* represent the metal and ceramic phases, respectively. The analysis focuses on a functionally graded doubly-curved nanoshell with *h* (thickness), where R_x and R_y denote the transverse and longitudinal curvature radii. The nanoshell experiences simultaneous exposure to uniform thermal and moisture fields. Four distinct geometric configurations are examined: hyperbolic ($R_x=a$, $R_y=-a$), ellipsoidal ($R_x=a$, $R_y=2a$), spherical ($R_x=R_y=a$), and cylindrical ($R_x\to\infty$, $R_y=a$) nanoshells, as illustrated in Fig. 1. The displacement components along the axial, circumferential, and transverse directions are designated as *u*, *v*, and *w*, respectively. To characterize the displacement field, Reddy's higher-order shear deformation theory is implemented, which inherently incorporates shear deformation effects without the need for empirical correction factors. The theoretical framework yields the following expression for the displacement field

$$u(x,y,z,t)=u_0(x,y,t)+(z-\frac{4z^3}{3h^2})\varphi_x(x,y,t)-\frac{4z^3}{3h^2}(\varphi_x+\frac{\partial w_0}{\partial x}), \tag{2}$$

$$v(x,y,z,t)=v_0(x,y,t)+(z-\frac{4z^3}{3h^2})\varphi_y(x,y,t)-\frac{4z^3}{3h^2}(\varphi_y+\frac{\partial w_0}{\partial y}), \tag{3}$$

$$w(x,y,z,t)=w_0(x,y,t). \tag{4}$$

The variables φ_x and φ_y correspond to the in-plane rotational displacements of the cross-section. Under these conditions, the strain components of the doubly-curved nanoshell may be expressed as

$$\begin{Bmatrix}\varepsilon_{xx}\\ \varepsilon_{yy}\\ \gamma_{xy}\end{Bmatrix}=\begin{Bmatrix}\varepsilon_{xx}^{(0)}\\ \varepsilon_{yy}^{(0)}\\ \gamma_{xy}^{(0)}\end{Bmatrix}+z\begin{Bmatrix}\varepsilon_{xx}^{(1)}\\ \varepsilon_{yy}^{(1)}\\ \gamma_{xy}^{(1)}\end{Bmatrix}+z^3\begin{Bmatrix}\varepsilon_{xx}^{(3)}\\ \varepsilon_{yy}^{(3)}\\ \gamma_{xy}^{(3)}\end{Bmatrix} \tag{5}$$

$$\begin{Bmatrix}\gamma_{xz}\\ \gamma_{yz}\end{Bmatrix}=\begin{Bmatrix}\gamma_{xz}^{(0)}\\ \gamma_{yz}^{(0)}\end{Bmatrix}+z^2\begin{Bmatrix}\gamma_{xz}^{(1)}\\ \gamma_{yz}^{(1)}\end{Bmatrix} \tag{6}$$

Here, ε_{xx},ε_{yy} and γ_{xy} stand for membrane strains, γ_{xz} and γ_{yz} are the transverse strains

$$\begin{Bmatrix}\varepsilon_{xx}^{(0)}\\ \varepsilon_{yy}^{(0)}\\ \gamma_{xy}^{(0)}\end{Bmatrix}=\begin{Bmatrix}\frac{\partial u_0}{\partial x}-\frac{w_0}{R_x}\\ \frac{\partial v_0}{\partial y}-\frac{w_0}{R_y}\\ \frac{\partial u_0}{\partial y}+\frac{\partial v_0}{\partial x}\end{Bmatrix},\begin{Bmatrix}\varepsilon_{xx}^{(1)}\\ \varepsilon_{yy}^{(1)}\\ \gamma_{xy}^{(1)}\end{Bmatrix}=\begin{Bmatrix}\frac{\partial \varphi_x}{\partial x}\\ \frac{\partial \varphi_y}{\partial y}\\ \frac{\partial \varphi_x}{\partial y}+\frac{\partial \varphi_y}{\partial x}\end{Bmatrix},\begin{Bmatrix}\varepsilon_{xx}^{(3)}\\ \varepsilon_{yy}^{(3)}\\ \gamma_{xy}^{(3)}\end{Bmatrix}=-\frac{4}{3h^2}\begin{Bmatrix}\frac{\partial \varphi_x}{\partial x}+\frac{\partial^2 w_0}{\partial x^2}\\ \frac{\partial \varphi_y}{\partial y}+\frac{\partial^2 w_0}{\partial y^2}\\ \frac{\partial \varphi_x}{\partial y}+\frac{\partial \varphi_y}{\partial x}+2\frac{\partial w_0}{\partial x}\frac{\partial w_0}{\partial y}\end{Bmatrix}, \tag{7}$$

$$\begin{Bmatrix}\gamma_{yz}^{(0)}\\ \gamma_{xz}^{(0)}\end{Bmatrix}=\begin{Bmatrix}\varphi_y+\frac{\partial w_0}{\partial y}\\ \varphi_x+\frac{\partial w_0}{\partial x}\end{Bmatrix},\begin{Bmatrix}\gamma_{yz}^{(2)}\\ \gamma_{xz}^{(2)}\end{Bmatrix}=-\frac{4}{3h^2}\begin{Bmatrix}\varphi_y+\frac{\partial w_0}{\partial y}\\ \varphi_x+\frac{\partial w_0}{\partial x}\end{Bmatrix}. \tag{8}$$

Hooke's law is a fundamental principle in solid mechanics that describes the linear elastic behavior of materials. It states that the stress applied to a material is directly proportional to the strain it produces, provided the material remains within its elastic limit. This relationship is mathematically expressed as

$$\left(1-l^2\nabla^2\right)\begin{bmatrix}\sigma_{xx}\\ \sigma_{yy}\\ \sigma_{xz}\\ \sigma_{yz}\\ \sigma_{xy}\end{bmatrix}=\left[1-(ea)^2\nabla^2\right]\begin{bmatrix}Q_{11} & Q_{12} & 0 & 0 & 0\\ Q_{12} & Q_{22} & 0 & 0 & 0\\ 0 & 0 & Q_{44} & 0 & 0\\ 0 & 0 & 0 & Q_{55} & 0\\ 0 & 0 & 0 & 0 & Q_{66}\end{bmatrix}\begin{bmatrix}\varepsilon_{xx}\\ \varepsilon_{yy}\\ \gamma_{xz}\\ \gamma_{yz}\\ \gamma_{xy}\end{bmatrix} \tag{9}$$

Herein, l is the strain gradient parameter, ea is the nonlocal parameter. And $Q_{11}=\frac{E_{11}}{1-v_{12}v_{21}}, Q_{22}=\frac{E_{22}}{1-v_{12}v_{21}}, Q_{12}=\frac{v_{21}E_{11}}{1-v_{12}v_{21}}, Q_{55}=Q_{44}=Q_{66}=G_{12}$. The resultant stresses are given as follows

$$\begin{bmatrix}N_x\\ N_y\\ N_{xy}\end{bmatrix}=\int_{-h/2}^{h/2}\begin{bmatrix}\sigma_x\\ \sigma_y\\ \sigma_{xy}\end{bmatrix}dz,\begin{bmatrix}M_x\\ M_y\\ M_{xy}\end{bmatrix}=\int_{-h/2}^{h/2}z\begin{bmatrix}\sigma_x\\ \sigma_y\\ \sigma_{xy}\end{bmatrix}dz,\begin{bmatrix}T_x\\ T_y\\ T_{xy}\end{bmatrix}=\int_{-h/2}^{h/2}z^3\begin{bmatrix}\sigma_x\\ \sigma_y\\ \sigma_{xy}\end{bmatrix}dz \tag{10}$$

$$\begin{bmatrix}Q_x\\ Q_y\end{bmatrix}=\int_{-h/2}^{h/2}\begin{bmatrix}\sigma_{xz}\\ \sigma_{yz}\end{bmatrix}dz,\begin{bmatrix}S_x\\ S_y\end{bmatrix}=\int_{-h/2}^{h/2}z^2\begin{bmatrix}\sigma_{xz}\\ \sigma_{yz}\end{bmatrix}dz. \tag{11}$$

In classical mechanics, Hamilton's principle serves as a powerful tool for deriving the equations that dictate the motion of a system. The principle is rooted in the idea that the actual path taken by a system is the one that minimizes the action, defined as the integral of the Lagrangian over time. Through the application of variational methods, this principle leads to the Euler-Lagrange equations, which are the differential equations governing the system's behavior

$$\left(1-l^2\nabla^2\right)\left\{\frac{\partial N_x}{\partial x}+\frac{\partial N_{xy}}{\partial y}\right\}=\left[1-(ea)^2\nabla^2\right]\left\{\overline{I}_1\frac{\partial^2 u_0}{\partial t^2}+\overline{I}_2\frac{\partial^2\varphi_x}{\partial t^2}-c_1\overline{I}_3\frac{\partial^3 w_0}{\partial x\partial t^2}\right\}, \tag{12}$$

$$\left(1-l^2\nabla^2\right)\left\{\frac{\partial N_{xy}}{\partial x}+\frac{\partial N_y}{\partial y}\right\}=\left[1-(ea)^2\nabla^2\right]\left\{\overline{I}_1^*\frac{\partial^2 v_0}{\partial t^2}+\overline{I}_2^*\frac{\partial^2\varphi_y}{\partial t^2}-c_1\overline{I}_3^*\right\}\frac{\partial^3 w_0}{\partial y\partial t^2}, \tag{13}$$

$$\begin{aligned}&\left(1-l^2\nabla^2\right)\left\{\frac{\partial Q_x}{\partial x}+\frac{\partial Q_y}{\partial y}+c_2\left(\frac{\partial S_x}{\partial x}+\frac{\partial S_y}{\partial y}\right)+c_1\left(\frac{\partial^2 T_x}{\partial x^2}+2\frac{\partial T_{xy}}{\partial x\partial y}+\frac{\partial^2 T_y}{\partial y^2}\right)+\frac{N_x}{R_x}+\frac{N_y}{R_y}+N_x\frac{\partial^2 w}{\partial x^2}\right.\\ &\left.+2N_{xy}\frac{\partial^2 w}{\partial x\partial y}+N_y\frac{\partial^2 w}{\partial y^2}+q\right\}=\left[1-(ea)^2\nabla^2\right]\left\{I_1\frac{\partial^2 w_0}{\partial t^2}+\overline{I}_3\frac{\partial^3 u_0}{\partial x\partial t^2}+\overline{I}_3^*\frac{\partial^3 v_0}{\partial y\partial t^2}+c_1\overline{I}_5\frac{\partial^3\varphi_x}{\partial x\partial t^2}\right.\\ &\left.+c_1\overline{I}_5^*\frac{\partial^3\varphi_y}{\partial y\partial t^2}-c_1^2 I_7\left(\frac{\partial^4 w_0}{\partial x^2\partial t^2}+\frac{\partial^4 w_0}{\partial y^2\partial t^2}\right)\right\},\end{aligned} \tag{14}$$

$$\begin{aligned}&\left(1-l^2\nabla^2\right)\left\{\frac{\partial M_x}{\partial x}+\frac{\partial M_{xy}}{\partial y}-Q_x+c_2S_x-c_1\left(\frac{\partial T_x}{\partial x}+\frac{\partial T_{xy}}{\partial y}\right)\right\}\\&=\left[1-(ea)^2\nabla^2\right]\left\{\overline{I}_2\frac{\partial^2 u_0}{\partial t^2}+\overline{I}_4\frac{\partial^2\varphi_x}{\partial t^2}-\overline{I}_5\frac{\partial^3 w_0}{\partial x\partial t^2}\right\},\end{aligned}\tag{15}$$

$$\begin{aligned}&\left(1-l^2\nabla^2\right)\left\{\frac{\partial M_{xy}}{\partial x}+\frac{\partial M_y}{\partial y}-Q_y+c_2S_y-c_1\left(\frac{\partial T_{xy}}{\partial x}+\frac{\partial T_y}{\partial y}\right)\right\}\\&=\left[1-(ea)^2\nabla^2\right]\left\{\overline{I}_2^*\frac{\partial^2 u_0}{\partial t^2}+\overline{I}_4^*\frac{\partial^2\varphi_x}{\partial t^2}-\overline{I}_5^*\frac{\partial^3 w_0}{\partial x\partial t^2}\right\}.\end{aligned}\tag{16}$$

Herein

$$\begin{aligned}&\left(1-l^2\nabla^2\right)\left\{A_{11}\frac{\partial^2 u}{\partial x^2}+A_{66}\frac{\partial^2 u}{\partial y^2}+A_{12}\frac{\partial^2 v}{\partial x\partial y}+A_{66}\frac{\partial^2 v}{\partial x\partial y}+\left(B_{11}-c_1E_{11}\right)\frac{\partial^2\varphi_x}{\partial x^2}\right.\\&\left.+\left(B_{66}-c_1E_{66}\right)\frac{\partial^2\varphi_x}{\partial y^2}-\left(\frac{A_{11}}{R_x}+\frac{A_{12}}{R_y}\right)\frac{\partial w}{\partial x}+\left[\left(B_{12}-c_1E_{12}\right)+\left(B_{66}-c_1E_{66}\right)\right]\frac{\partial^2\varphi_y}{\partial x\partial y}\right\}\\&=\left[1-(ea)^2\nabla^2\right]\left\{\overline{I}_1\frac{\partial^2 u}{\partial t^2}+\overline{I}_2\frac{\partial\varphi_x}{\partial t^2}-c_1\overline{I}_3\frac{\partial^3 w}{\partial x\partial t^2}\right\},\end{aligned}\tag{17}$$

$$\begin{aligned}&\left(1-l^2\nabla^2\right)\left\{\left(A_{12}+A_{66}\right)\frac{\partial^2 u}{\partial x\partial y}+A_{66}\frac{\partial^2 v}{\partial x^2}+A_{22}\frac{\partial^2 v}{\partial y^2}-\frac{A_{22}}{R_y}+B_{12}\frac{\partial^2\varphi_x}{\partial x\partial y}\right.\\&-c_1E_{12}\frac{\partial^2\varphi_x}{\partial x\partial y}+B_{66}\left(\frac{\partial^2\varphi_x}{\partial x\partial y}+\frac{\partial^2\varphi_y}{\partial x^2}\right)-c_1E_{66}\left(\frac{\partial^2\varphi_x}{\partial x\partial y}+\frac{\partial^2\varphi_y}{\partial x^2}\right)\\&\left.+\left(B_{22}-c_1E_{22}\right)\frac{\partial^2\varphi_y}{\partial y^2}-\frac{A_{12}}{R_x}\frac{\partial w}{\partial y}\right\}=\left[1-(ea)^2\nabla^2\right]\left\{\overline{I}_1^*\frac{\partial^2 v}{\partial t^2}+\overline{I}_2^*\frac{\partial\varphi_y}{\partial t^2}-c_1\overline{I}_3^*\frac{\partial^3 w}{\partial y\partial t^2}\right\},\end{aligned}\tag{18}$$

$$\begin{aligned}&\left(1-l^2\nabla^2\right)\left\{c_1\left(E_{11}\frac{\partial^3 u}{\partial x^3}+E_{12}\frac{\partial^3 u}{\partial x\partial y^2}+2E_{66}\frac{\partial^3 u}{\partial x\partial y^2}\right)+\frac{A_{11}}{R_x}\frac{\partial u}{\partial x}+\frac{A_{12}}{R_y}\frac{\partial u}{\partial x}+c_1\left(E_{22}\frac{\partial^3 v}{\partial y^3}+E_{12}\frac{\partial^3 v}{\partial x^2\partial y}\right)\right.\\&+2c_1E_{66}\frac{\partial^3 v}{\partial x^2\partial y}+\left(A_{55}+2c_2D_{55}+c_2^2F_{55}-\frac{c_1E_{11}}{R_x}\right)\frac{\partial^2 w}{\partial x^2}-\left(\frac{A_{11}}{R_x^2}+\frac{2A_{12}}{R_xR_y}+\frac{A_{22}}{R_y^2}\right)w\\&+\left(A_{44}+2c_2D_{44}+c_2^2F_{44}-\frac{c_1E_{22}}{R_y}\right)\frac{\partial^2 w}{\partial y^2}+\frac{A_{22}}{R_y}\frac{\partial v}{\partial y}+\frac{A_{12}}{R_x}\frac{\partial v}{\partial y}+\left(2c_2D_{55}+c_2^2F_{55}\frac{\partial\varphi_x}{\partial x}+\frac{B_{11}}{R_x}+\frac{B_{12}}{R_y}-\frac{c_1E_{11}}{R_x}\right)\frac{\partial\varphi_x}{\partial x}\\&+\left(A_{55}-\frac{c_1E_{12}}{R_y}\right)\frac{\partial\varphi_x}{\partial x}+\left(c_1F_{11}-c_1^2H_{11}\right)\frac{\partial^3\varphi_x}{\partial x^3}+\left(c_1F_{12}+2c_1F_{66}-2c_1^2H_{66}-c_1^2H_{12}\right)\frac{\partial^3\varphi_x}{\partial x\partial y^2}\\&\left.+\left(2c_2D_{44}+c_2^2F_{44}+\frac{B_{12}}{R_x}+\frac{B_{22}}{R_y}-\frac{c_1E_{12}}{R_x}-\frac{c_1E_{22}}{R_y}+A_{44}\right)\frac{\partial\varphi_y}{\partial y}+\left(c_1F_{22}-c_1^2H_{22}\right)\frac{\partial^3\varphi_y}{\partial y^3}\right.\end{aligned}$$

$$
\begin{aligned}
&+\left(c_1F_{12}+2c_1F_{66}-2c_1^2H_{66}-c_1^2H_{12}\right)\frac{\partial^3\varphi_y}{\partial x^2\partial y}+q\Bigg\}\\
&=\left[1-(ea)^2\nabla^2\right]\left\{I_1\frac{\partial^2 w}{\partial t^2}+\overline{I}_3\frac{\partial^3 u}{\partial x\partial t^2}+\overline{I}_3^*\frac{\partial^3 v}{\partial y\partial t^2}+c_1\overline{I}_5\frac{\partial^3\varphi_x}{\partial x\partial t^2}+c_1\overline{I}_5^*\frac{\partial^3\varphi_y}{\partial y\partial t^2}-c_1^2I_7\left(\frac{\partial^4 w}{\partial x^2\partial t^2}+\frac{\partial^4 w}{\partial y^2\partial t^2}\right)\right\},
\end{aligned}
\tag{19}
$$

$$
\begin{aligned}
&\left(1-l^2\nabla^2\right)\Bigg\{\left(B_{11}-c_1E_{11}\right)\frac{\partial^2 u}{\partial x^2}+\left(B_{66}-c_1E_{66}\right)\frac{\partial^2 u}{\partial y^2}+\left(B_{12}-c_1E_{12}\right)\frac{\partial^2 v}{\partial x\partial y}+\left(B_{66}-c_1E_{66}\right)\frac{\partial^2 v}{\partial x\partial y}\\
&-\left(A_{55}-c_2^2F_{55}-c_1\frac{E_{11}}{R_x}-c_1\frac{E_{12}}{R_y}+\frac{B_{11}}{R_x}+\frac{B_{12}}{R_y}\right)\frac{\partial w}{\partial x}+2c_1F_{66}\frac{\partial^2\varphi_y}{\partial x\partial y}+\left(D_{11}-2c_1F_{11}+c_1^2H_{11}\right)\frac{\partial^2\varphi_x}{\partial x^2}\\
&+\left(D_{66}-2c_1F_{66}+c_1^2H_{66}\right)\frac{\partial^2\varphi_x}{\partial y^2}-\left(A_{55}-c_2^2F_{55}\right)\varphi_x\Bigg\}\\
&+\left(D_{12}-2c_1F_{12}+c_1^2H_{12}+D_{66}\right)\frac{\partial^2\varphi_y}{\partial x\partial y}-c_1^2H_{66}\frac{\partial^2\varphi_y}{\partial x\partial y}\Bigg\}\\
&=\left[1-(ea)^2\nabla^2\right]\left\{\overline{I}_2\frac{\partial^2 u}{\partial t^2}+\overline{I}_4\frac{\partial^2\varphi_x}{\partial t^2}-\overline{I}_5\frac{\partial^3 w}{\partial x\partial t^2}\right\},
\end{aligned}
\tag{20}
$$

$$
\begin{aligned}
&\left(1-l^2\nabla^2\right)\Bigg\{\left(B_{12}-c_1E_{12}+B_{66}-c_1E_{66}\right)\frac{\partial^2 u}{\partial x\partial y}+\left(B_{66}-c_1E_{66}\right)\frac{\partial^2 v}{\partial x^2}+\left(B_{22}-c_1E_{22}\right)\frac{\partial^2 v}{\partial y^2}+\frac{B_{12}}{R_x}\frac{\partial w}{\partial y}\\
&-\left(A_{44}-c_2^2F_{44}-c_1\frac{E_{12}}{R_x}-c_1\frac{E_{22}}{R_y}\right)\frac{\partial w}{\partial y}+c_1^2H_{12}\frac{\partial^2\varphi_x}{\partial x\partial y}+D_{66}\frac{\partial^2\varphi_x}{\partial x\partial y}+\left(D_{22}-2c_1F_{22}+c_1^2H_{22}\right)\frac{\partial^2\varphi_y}{\partial y^2}\\
&+\left(D_{12}-2c_1F_{12}-2c_1F_{66}+c_1^2H_{66}\right)\frac{\partial^2\varphi_x}{\partial x\partial y}+\left(D_{66}+c_1^2H_{66}\right)\frac{\partial^2\varphi_y}{\partial x^2}\\
&-2c_1F_{66}\frac{\partial^2\varphi_y}{\partial x^2}-A_{55}\varphi_y+\frac{B_{22}}{R_y}\frac{\partial w}{\partial y}-c_2^2F_{44}\varphi_y\Bigg\}=\left[1-(ea)^2\nabla^2\right]\left\{\overline{I}_2^*\frac{\partial^2 v}{\partial t^2}+\overline{I}_4^*\frac{\partial^2\varphi_y}{\partial t^2}-\overline{I}_5^*\frac{\partial^3 w}{\partial y\partial t^2}\right\}.
\end{aligned}
\tag{21}
$$

in which

$$
\begin{aligned}
&\overline{I}_1=I_1+\frac{2I_2}{R_x},\ \overline{I}_1^*=I_1+\frac{2I_2}{R_y},\overline{I}_2=I_2+\frac{I_3}{R_x}-c_1I_4-c_1\frac{I_5}{R_x},\\
&\overline{I}_2^*=I_2+\frac{I_3}{R_y}-c_1I_4-c_1\frac{I_5}{R_y},\overline{I}_3=c_1I_4+c_1\frac{I_5}{R_x},\overline{I}_3^*=c_1I_4+c_1\frac{I_5}{R_y},\\
&\overline{I}_4=I_3-2c_1I_5+c_1^2I_7,\ \overline{I}_4^*=I_3-2c_1I_5+c_1^2I_7,\\
&\overline{I}_5=c_1I_5-c_1^2I_7,\ \overline{I}_5^*=c_1I_5-c_1^2I_7.
\end{aligned}
\tag{22}
$$

with, $\{I_1,I_2,I_3,I_4,I_5,I_7\}=\int_{-h/2}^{h/2}\rho(z)\{1,z,z^2,z^3,z^4,z^6\}\mathrm{d}z$.

When analyzing the propagation of elastic waves in functionally graded (FG) nanoshells, it is necessary to determine a solution to the governing Eqs. (17)-(21) that adheres to the specified boundary conditions. To achieve this, the displacement shape function is selected following the methodology.

For four clamped boundary conditions (CCCC)

$$u_0(x,y,t)=\sum_{m,n=1,3,5...}^{\infty}u_{mn}\frac{\mathrm{d}}{dx}\left[\cos^2(\frac{m\pi x}{a})\right]\sin^2\left(\frac{n\pi y}{b}\right)(e^{\mathrm{i}(\kappa_1 x+\kappa_2 y+\omega t)}+e^{\mathrm{i}(\kappa_1 x+\kappa_2 y-\omega t)}) \tag{23}$$

$$v_0(x,y,t)=\sum_{m,n=1,3,5...}^{\infty}v_{mn}\cos^2(\frac{m\pi x}{a})\frac{d}{dy}\left[\sin^2\left(\frac{n\pi y}{b}\right)\right](e^{\mathrm{i}(\kappa_1 x+\kappa_2 y+\omega t)}+e^{\mathrm{i}(\kappa_1 x+\kappa_2 y-\omega t)}) \tag{24}$$

$$w_0(x,y,t)=\sum_{m,n=1,3,5...}^{\infty}w_{mn}\sin^2(\frac{m\pi x}{a})\sin^2\left(\frac{n\pi y}{b}\right)(e^{\mathrm{i}(\kappa_1 x+\kappa_2 y+\omega t)}+e^{\mathrm{i}(\kappa_1 x+\kappa_2 y-\omega t)}) \tag{25}$$

$$\varphi_x(x,y,t)=\sum_{m,n=1,3,5...}^{\infty}\varphi_{mn}^{x}\frac{\mathrm{d}}{dx}\left[\cos^2(\frac{m\pi x}{a})\right]\sin^2\left(\frac{n\pi y}{b}\right)(e^{\mathrm{i}(\kappa_1 x+\kappa_2 y+\omega t)}+e^{\mathrm{i}(\kappa_1 x+\kappa_2 y-\omega t)}) \tag{26}$$

$$\varphi_y(x,y,t)=\sum_{m,n=1,3,5...}^{\infty}\varphi_{mn}^{y}\cos^2(\frac{m\pi x}{a})\frac{d}{dy}\left[\sin^2\left(\frac{n\pi y}{b}\right)\right](e^{\mathrm{i}(\kappa_1 x+\kappa_2 y+\omega t)}+e^{\mathrm{i}(\kappa_1 x+\kappa_2 y-\omega t)}) \tag{27}$$

For four edges simply supported (SSSS)

$$u_0(x,y,t)=\sum_{m,n=1,3,5...}^{\infty}u_{mn}\cos(\frac{m\pi x}{a})\sin\left(\frac{n\pi y}{b}\right)(e^{\mathrm{i}(\kappa_1 x+\kappa_2 y+\omega t)}+e^{\mathrm{i}(\kappa_1 x+\kappa_2 y-\omega t)}) \tag{28}$$

$$v_0(x,y,t)=\sum_{m,n=1,3,5...}^{\infty}v_{mn}\sin(\frac{m\pi x}{a})\cos\left(\frac{n\pi y}{b}\right)(e^{\mathrm{i}(\kappa_1 x+\kappa_2 y+\omega t)}+e^{\mathrm{i}(\kappa_1 x+\kappa_2 y-\omega t)}) \tag{29}$$

$$w_0(x,y,t)=\sum_{m,n=1,3,5...}^{\infty}w_{mn}\sin(\frac{m\pi x}{a})\sin\left(\frac{n\pi y}{b}\right)(e^{\mathrm{i}(\kappa_1 x+\kappa_2 y+\omega t)}+e^{\mathrm{i}(\kappa_1 x+\kappa_2 y-\omega t)}) \tag{30}$$

$$\varphi_x(x,y,t)=\sum_{m,n=1,3,5...}^{\infty}\varphi_{mn}^{x}\cos(\frac{m\pi x}{a})\sin\left(\frac{n\pi y}{b}\right)(e^{\mathrm{i}(\kappa_1 x+\kappa_2 y+\omega t)}+e^{\mathrm{i}(\kappa_1 x+\kappa_2 y-\omega t)}) \tag{31}$$

$$\varphi_y(x,y,t)=\sum_{m,n=1,3,5...}^{\infty}\varphi_{mn}^{y}\sin(\frac{m\pi x}{a})\cos\left(\frac{n\pi y}{b}\right)(e^{\mathrm{i}(\kappa_1 x+\kappa_2 y+\omega t)}+e^{\mathrm{i}(\kappa_1 x+\kappa_2 y-\omega t)}) \tag{32}$$

For the cantilever boundary condition (CCFF),

$$u_0(x,y,t)=\sum_{m,n=1,3,5...}^{\infty}u_{mn}\sin\frac{m\pi x}{2a}\cos\frac{n\pi y}{b}(e^{\mathrm{i}(\kappa_1 x+\kappa_2 y+\omega t)}+e^{\mathrm{i}(\kappa_1 x+\kappa_2 y-\omega t)}) \tag{33}$$

$$v_0(x,y,t)=\sum_{m,n=1,3,5...}^{\infty}v_{mn}\sin\frac{m\pi x}{2a}\sin\frac{n\pi y}{b}(e^{\mathrm{i}(\kappa_1 x+\kappa_2 y+\omega t)}+e^{\mathrm{i}(\kappa_1 x+\kappa_2 y-\omega t)}) \tag{34}$$

$$w_0(x,y,t)=\sum_{m,n=1,3,5...}^{\infty} w_{mn}X_m(x)Y_n(y)(e^{\mathrm{i}(\kappa_1 x+\kappa_2 y+\omega t)}+e^{\mathrm{i}(\kappa_1 x+\kappa_2 y-\omega t)}) \tag{35}$$

$$\varphi_x(x,y,t)=\sum_{m,n=1,3,5...}^{\infty} \varphi_{mn}^{x}\sin\frac{m\pi x}{2a}\cos\frac{n\pi y}{b}(e^{\mathrm{i}(\kappa_1 x+\kappa_2 y+\omega t)}+e^{\mathrm{i}(\kappa_1 x+\kappa_2 y-\omega t)}) \tag{36}$$

$$\varphi_y(x,y,t)=\sum_{m,n=1,3,5...}^{\infty} \varphi_{mn}^{y}\left(1-\cos\frac{m\pi x}{2a}\right)\sin\frac{n\pi y}{b}(e^{\mathrm{i}(\kappa_1 x+\kappa_2 y+\omega t)}+e^{\mathrm{i}(\kappa_1 x+\kappa_2 y-\omega t)}) \tag{37}$$

Herein

$$\begin{aligned}
&X_m(x)=\sin\frac{\lambda_m x}{2a}-\sinh\frac{\lambda_m x}{2a}+\alpha_m(\cosh\frac{\lambda_m x}{2a}-\cos\frac{\lambda_m x}{2a})\\
&Y_n(y)=\sin\frac{\mu_n y}{2b}+\sinh\frac{\mu_n y}{2b}-\beta_n(\cosh\frac{\mu_n y}{2b}+\cos\frac{\mu_n y}{2b})\\
&\alpha_m=\frac{\sinh\lambda_m+\sin\lambda_m}{\cosh\lambda_m+\cos\lambda_m},\beta_j=\frac{\sinh\mu_n-\sin\mu_n}{\cosh\mu_n-\cos\mu_n}\\
&\cos\lambda_m\cosh\lambda_m+1=0,\cos\mu_n\cosh\mu_n-1=0.
\end{aligned} \tag{38}$$

It is important to note that in Eqs. (23)-(37), the parameters $u_{mn}, v_{mn}, w_{mn}, \phi_{mn}^{x}$ and ϕ_{mn}^{y} represent wave amplitudes, while k_1 and k_2 denote the wave numbers along the x- and y-directions, respectively. Additionally, ω corresponds to the circular frequency. To derive the governing equations, we substitute the expressions from Eqs. (23)-(37) into the system of Eqs. (17)-(21). Subsequently, by applying the Galerkin principle and leveraging the orthogonality conditions of the mode functions, a series of mathematical operations are performed. For the sake of analytical simplicity and computational efficiency, our analysis focuses exclusively on the fundamental mode, where m=n=1. This simplification allows us to reduce the complexity of the problem while retaining essential physical insights. As a result of these steps, a characteristic equation in terms of the eigenvalue is obtained. This eigenvalue equation plays a pivotal role in determining the dynamic response of the system, providing critical information about its stability and vibrational behavior, through a series of mathematical derivations, the following expression is derived.

$$(\boldsymbol{K}-\omega^2\boldsymbol{M})[u_{11},v_{11},w_{11},\varphi_{11}^{x},\varphi_{11}^{y}]^{\mathrm{T}}=0 \tag{39}$$

If the equation is to have a non-zero solution, it must have: solution where not all variables are zero, it is essential that the equation must satisfy (Karami *et al*. 2018)

$$\left|\boldsymbol{K}-\omega^2\boldsymbol{M}\right|=0 \tag{40}$$

The formulation in Eq. (40) outlines the definitions of the stiffness matrix and the mass matrix, as detailed subsequently

$$\boldsymbol{K}=\begin{bmatrix}
k_{11} & k_{12} & k_{13} & k_{14} & k_{15}\\
k_{21} & k_{22} & k_{23} & k_{24} & k_{25}\\
k_{31} & k_{32} & k_{33} & k_{34} & k_{35}\\
k_{41} & k_{42} & k_{43} & k_{44} & k_{45}\\
k_{51} & k_{52} & k_{53} & k_{54} & k_{55}
\end{bmatrix} \tag{41}$$

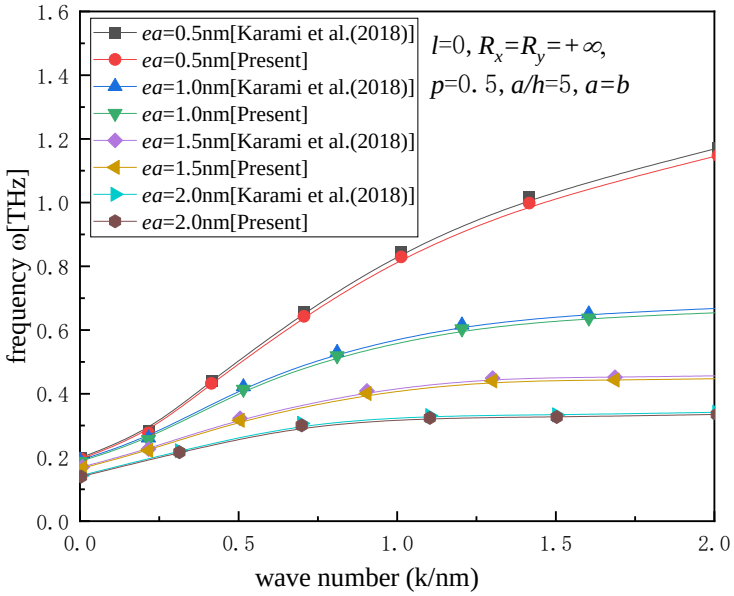

Fig. 2 Comparison of current phase velocities with those from Karami *et al.* (2018) for CCCC

$$\boldsymbol{M} = (1+ea^2(\kappa_1^{\,2}+\kappa_2^{\,2}))\begin{bmatrix} I_0 & 0 & 0 & 0 & 0 \\ 0 & I_0 & 0 & 0 & 0 \\ 0 & 0 & 9I_0 & 0 & 0 \\ 0 & 0 & 0 & 3I_2 & 0 \\ 0 & 0 & 0 & 0 & 3I_2 \end{bmatrix} \tag{42}$$

The dispersion relation (40) yields five distinct pairs of real solutions, each corresponding to a unique wave mode. Among these, the smallest root is associated with the bending wave. Given the material's isotropic properties—meaning its mechanical behavior is identical along the *x*- and *y*-axes—the phase velocity (C_p) can be determined using the relation $\omega=k\cdot C_p$, where ω is the angular frequency and k is the wavenumber, and $k=\kappa_1=\kappa_2$. Similarly, the group velocity (C_g) can be derived from the dispersion relation by taking the derivative of ω with respect to k, i.e., $C_g=d\omega/dk$.

3. Results and discussion

To comprehensively validate the accuracy and reliability of this research, the FG nanoplates are systematically examined under conditions where the strain gradient parameter is intentionally disregarded. This is achieved by setting the strain gradient parameter l to zero. The material properties and geometric dimensions are meticulously aligned with those referenced in established prior studies (Karami *et al.* 2018). For a direct and quantitative comparison, Fig. 2 displays the curve between the frequency and the wave number respectively, as reported by Karami *et al.* (2018). The comparative analysis reveals an excellent agreement, where our computational findings, represented by discrete data points, closely match their continuous linear results. This high degree of concordance serves as a robust verification of the correctness and validity of the

Table 2 The relationship between wave number and frequency of bending waves

k	ω (Hz) (present)	ω (Hz) (Karami *et al.* 2019)
0.1	2.398275	2.4225
1	2.2644384	2.2827
2	2.0501478	2.0646
5	2.0120196	2.0201
10	1.4808612	1.4898

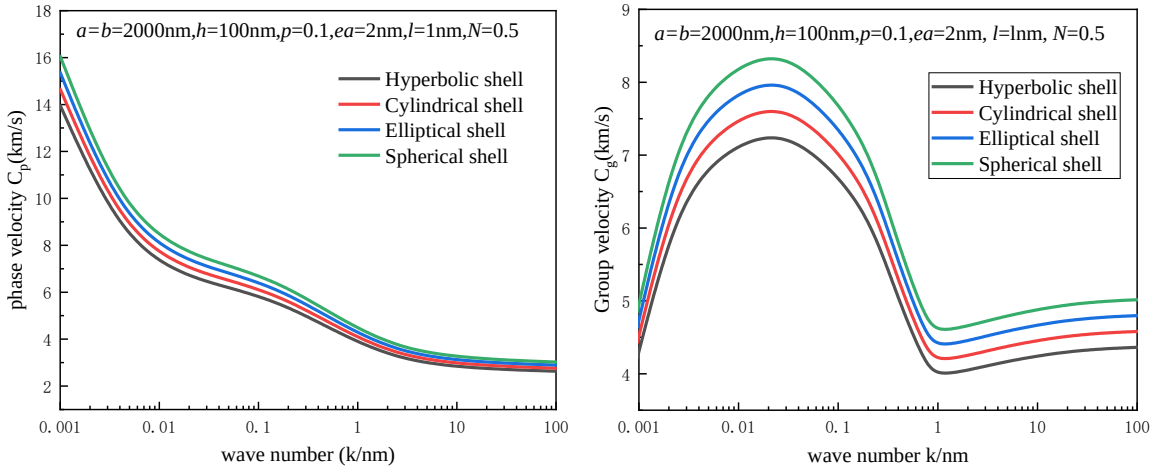

(a) (b)

Fig. 3 (a) Phase velocity and (b) Group velocity diagrams for different shell types (CCCC)

present theoretical model and computational methodology.

To validate the accuracy of this paper, Table 2 analyzes the relationship between wave number and frequency of bending waves, exploring the influence of different parameters on the wave characteristics of doubly-curved spherical nanoshells. This section focuses on the effects of nonlocal and strain gradient parameters on the frequency of doubly-curved nanoshells, with shell geometric parameters set as (R_x=R_y=50 h, l=0.2, ea=0.5). Comparative analysis confirms the validity of this paper.

For all subsequent parametric analyses, the material system is defined using more contemporary and high-performance materials. The characteristics are specified as follows: Silicon Nitride (Si_3N_4) with a ceramic elastic modulus E_c=322.27 GPa, density ρ_c=2307 kg/m³, and Poisson's ratio υ_c=0.24; and Stainless Steel (SUS304) with a metallic elastic modulus E_m=207.79 GPa, density ρ_m=8166 kg/m³, and Poisson's ratio υ_m=0.24. and for hyperbolic (R_x=a, R_y=-a), ellipsoidal (R_x=a, R_y=2a), spherical (R_x=R_y=a), and cylindrical (R_x→∞, R_y=a) nanoshells, a=2000 nm. To maintain a focused scope, the subsequent study concentrates exclusively on the behavior of the bending (or flexural) waves, which are fundamental to the dynamic response of plate structures.

Fig. 3 investigates the influence of different shell types on phase velocity and group velocity. Of the four shell geometries compared, the hyperbolic shell consistently shows the lowest values for both phase and group velocities. The spherical shell ranks highest in both categories, while the

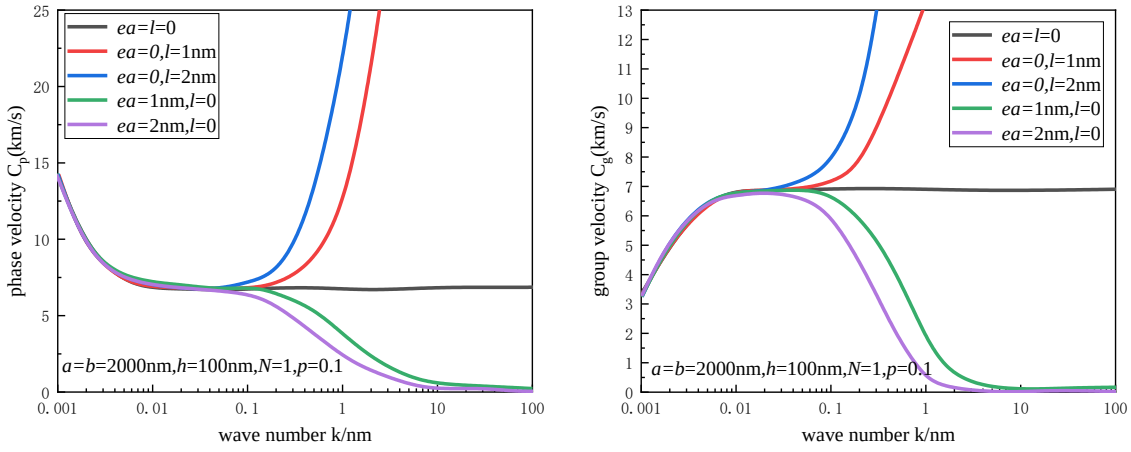

Fig. 4 Effect of the nonlocal parameter (*ea*) and the strain gradient parameter (*l*) on the (a) phase velocity and (b) group velocity for spherical shells (CCCC)

cylindrical and ellipsoidal shells occupy intermediate positions in this ascending order. Specially, in Fig. 3(a), it can be observed that, arranged in ascending order, the hyperbolic shell exhibits the lowest phase velocity, followed by the cylindrical shell, then the ellipsoidal shell, and finally the spherical shell. Similarly, in Fig. 3(b), the hyperbolic shell demonstrates the smallest group velocity, followed by the cylindrical shell, the ellipsoidal shell, and the spherical shell. This phenomenon arises because the geometric curvature of the shell directly affects the propagation path and energy distribution of elastic waves. The negative Gaussian curvature of the hyperbolic shell causes significant wavefront distortion, increasing the tortuosity of the propagation path and thereby reducing both phase and group velocities. In contrast, the positive Gaussian curvature of the spherical shell results in a more uniform wave propagation path with lower energy dissipation, leading to higher velocities. Additionally, the stiffness of the shell (related to thickness and material properties) is positively correlated with elastic wave speed. Hyperbolic shells often require more complex structural designs to achieve negative curvature, which may result in lower local stiffness and reduced wave speed. The spherical shell's symmetry ensures a more uniform stiffness distribution, facilitating higher wave speeds. Furthermore, curvature variations alter the dispersion characteristics of waves. The strong curvature gradient of the hyperbolic shell may exacerbate dispersion effects, reducing group velocity, while the smooth curvature of the spherical shell results in weaker dispersion and more stable group velocities. These combined factors lead to the hyperbolic shell having the lowest phase and group velocities, with the cylindrical and ellipsoidal shells in between, and the spherical shell achieving the highest speeds. This pattern reflects the comprehensive impact of geometric curvature on elastic wave propagation.

The influence of intrinsic size parameters on wave propagation characteristics is thoroughly investigated in Fig. 4. These figures respectively illustrate the effect of the nonlocal parameter (*ea*) and the strain gradient parameter (*l*) on the phase velocity and group velocity of porous functionally graded doubly curved nanoshells. The data conclusively indicate that in the regime of very small wave numbers (i.e., long wavelengths), these size parameters exert a negligible influence on the dispersion relationship. This can be attributed to the fact that at long wavelengths, the wave "feels" the structure as a homogeneous continuum, and the micro-structural details

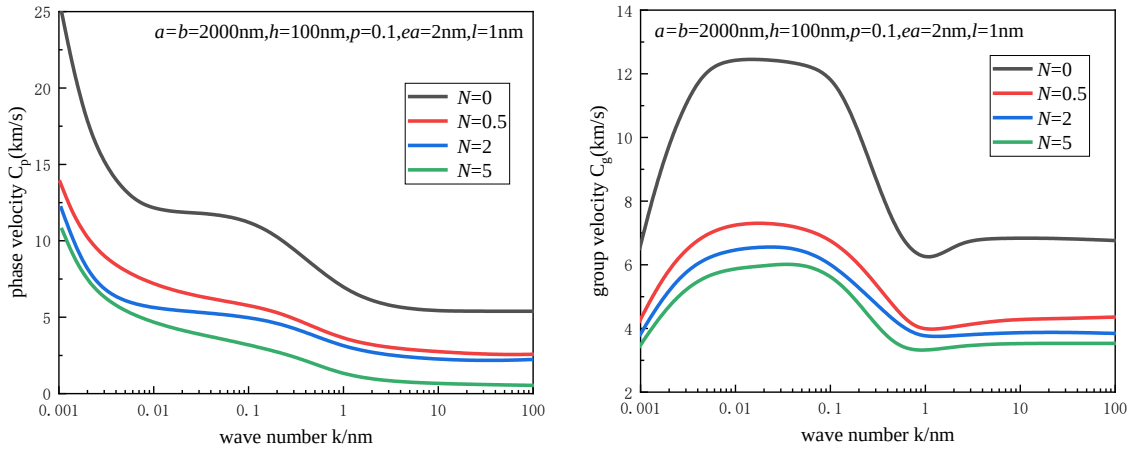

(a) (b)

Fig. 5 Effect of the power-law index (*N*) on the (a) phase velocity and (b) group velocity for spherical shells (CCCC)

captured by '*ea*' and '*l*' become irrelevant. Conversely, when the wave number is relatively large (i.e., short wavelengths), both the phase velocity and the group velocity are markedly and non-trivially affected. This significant impact arises because short-wavelength waves are highly sensitive to the local microstructure and internal length scales of the material. The nonlocal parameter, which accounts for long-range atomic interactions, introduces a stiffness-softening effect, typically leading to a decrease in wave velocities. In contrast, the strain gradient parameter, which embodies the energy associated with spatial variations in strain, contributes to a stiffness-hardening mechanism, often resulting in an increase in wave velocities, especially at high wave numbers. The observed interplay and the condition that size effects become prominent only with substantial parameter values are fully consistent with the conclusions drawn in the existing literature on nonlocal strain gradient theory.

Furthermore, the impact of the power-law index (*N*), which governs the gradation of material properties through the doubly curved nanoshell's thickness, is examined in Fig. 5. The results demonstrate a consistent and pronounced declining trend in both phase and group velocities as *N* increases. The primary reason for this behavior is the associated reduction in the volume fraction of the stiffer ceramic phase (Si_3N_4). A higher *N* value implies a richer metallic constituent (SUS304), which possesses a lower elastic modulus compared to the ceramic. This reduction in the effective elastic modulus directly leads to a decrease in the overall stiffness of the doubly curved nanoshell. Since wave propagation velocities are fundamentally proportional to the square root of the stiffness-to-density ratio, the reduced stiffness consequently results in lower phase and group velocities, despite the concurrent change in effective density.

Similarly, the effect of introducing porosity is analyzed in Fig. 6, which shows that an increase in the pore volume fraction (*p*) also leads to a significant reduction in both phase and group velocities. The underlying mechanisms for this reduction are twofold. Firstly, the presence of pores creates discontinuities in the solid material, effectively reducing the load-bearing cross-sectional area and hence the overall effective stiffness of the doubly curved nanoshell, which is a primary factor controlling wave speed. Secondly, the introduction of pores generally decreases the effective mass density of the material. However, the detrimental effect of porosity on stiffness

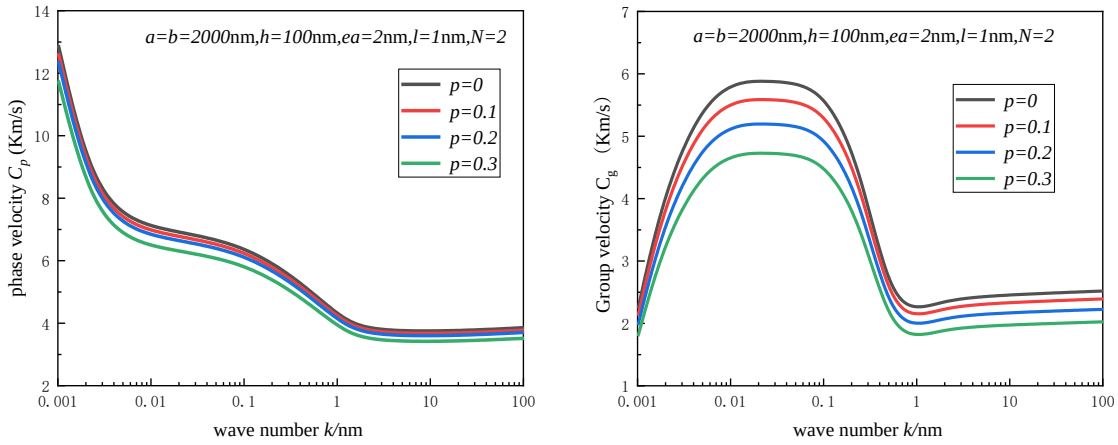

(a) (b)

Fig. 6 Effect of the pore volume fraction (p) on the (a) phase velocity and (b) group velocity for spherical shells (CCCC)

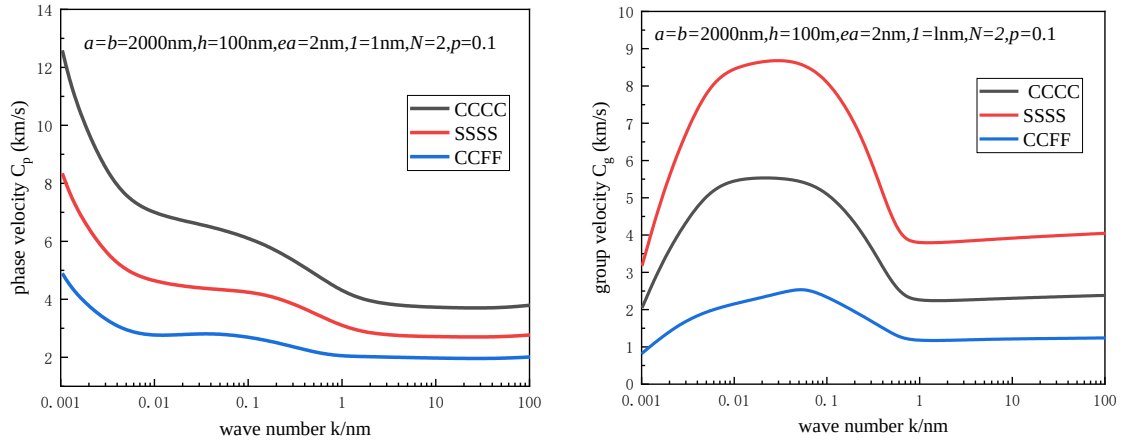

(a) (b)

Fig. 7 Effect of the different boundary conditions on the (a) phase velocity and (b) group velocity for spherical shells

typically outweighs the effect of the reduced density (the stiffness often degrades faster than the density), leading to a net decrease in the wave velocities. This makes the control of porosity a critical factor in tailoring the dynamic performance of FG doubly curved nanoshells for specific engineering applications.

Fig. 7 investigates the influence of different boundary conditions (CCCC, SSSS, CCFF) on the phase and group velocities of doubly curved nanoshells. As shown in the figure, the CCCC exhibits the highest phase velocity. This is because the rigidly fixed boundary conditions constrain the free vibration of the plate, thereby enhancing its bending stiffness and consequently increasing the wave speed. In contrast, the CCFF plate demonstrates the lowest phase velocity, as the free-edge boundary conditions significantly reduce the effective stiffness of the structure, leading to a decrease in wave speed. The SSSS plate has a phase velocity between these two cases, as the

simply-supported boundary conditions impose less constraint on stiffness compared to the clamped boundaries. Regarding group velocity, the SSSS plate exhibits the highest group velocity. The SSSS allows the plate to vibrate more freely, resulting in higher energy propagation efficiency. The CCCC has a lower group velocity, as the CCCC partially suppresses the energy transfer of certain vibration modes. The CCFF has the smallest group velocity, as the free-edge boundary causes significant energy dispersion, leading to a substantial reduction in group velocity. In summary, the CCCC enhances structural stiffness, increasing phase velocity but potentially suppressing group velocity. In contrast, the SSSS supports more vibration modes, which is beneficial for improving group velocity. The clamped plate's vibration modes are more restricted, thus limiting its group velocity.

4. Conclusions

Based on the NSGT framework and accounting for the moment of inertia, the governing equations of motion are derived for porous FG doubly curved shells. The Galerkin method is then applied to eliminate the spatial variables from the partial differential equation system, transforming it into an ordinary differential equation in the time domain. By applying the boundary conditions and solving the characteristic equation, the dispersion characteristics of porous FG strain gradient doubly curved shells are obtained:

(1) The phase and group velocities increase with shell curvature: hyperbolic (lowest), cylindrical, ellipsoidal, and spherical (highest). Negative curvature in hyperbolic shells distorts wave paths, increasing tortuosity and reducing speed, while spherical shells' positive curvature enables uniform propagation with less dispersion and higher stiffness, enhancing wave velocities.

(2) The size parameters (nonlocal *ea* and strain gradient *l*) significantly affect wave propagation in porous FG nanoshells only at high wave numbers (short wavelengths), with *ea* reducing velocities (stiffness-softening) and *l* increasing them (stiffness-hardening), while their influence is negligible at low wave numbers (long wavelengths), consistent with nonlocal strain gradient theory.

(3) Increasing the power-law index reduces phase and group velocities in doubly curved nanoshells. This occurs because higher *N* values increase the softer metallic (SUS304) fraction, lowering effective stiffness. Since wave speeds depend on the square root of stiffness-to-density ratio, the reduced stiffness leads to slower wave propagation.

(4) The CCCC plate achieves the highest phase velocity due to enhanced stiffness, while the CCFF plate shows the lowest. For group velocity, the SSSS plate excels in energy propagation, whereas the CCCC and CCFF plates exhibit lower efficiency due to boundary constraints and energy dispersion, respectively. Thus, boundary conditions critically influence wave propagation characteristics in doubly curved nanoshells.

These findings have direct applications in the design of next-generation MEMS/NEMS devices. The identified relationship between geometry and wave speed can guide the selection of shell curvature for specific functions, such as using hyperbolic shells as delay lines and spherical shells for high-speed signal channels. Furthermore, the effects of size parameters and material gradation provide key principles for tuning the performance of nano-resonators and ultrasensitive mass sensors. The analysis of boundary conditions also offers crucial insights for optimizing energy transmission in integrated nano-acoustic systems.

Acknowledgement

The Natural Science Foundation of Hunan Province (2024JJ8100); Scientific research project of Hunan Provincial Department of Education (24B0974 and 22B0956); and Xiangtan science and technology planning project (CG-YB20240004) are acknowledged.

References

Ardalani, A.R.A., Amiri, A. and Talebitooti, R. (2022), "On size-dependent wave propagation of flexoelectric nanoshells interacted with internal moving fluid flow", *Wave. Random Complex Media*, **34**(6), 6210-6239. https://doi.org/10.1080/17455030.2021.2018152.

Benadouda, M., Bourouis, M.E., Dahmane, M., Bennai, R., Atmane, H.A. and Safer, O. (2025), "Dynamic response of wave propagation in functionally graded beams with defects: effects of porosity and cracks", *Acta Mechanica*, **236**(3), 2279-2296. https://doi.org/10.1007/s00707-025-04270-4.

Bennai, R., Atmane, R.A., Bernard, F., Nebab, M., Mahmoudi, N., Atmane, H.A., Aldosari, S.M. and Tounsi, A. (2022a), "Study on stability and free vibration behavior of porous FGM beams", *Steel Compos. Struct.*, **45**(1), 67-82. https://doi.org/10.12989/scs.2022.45.1.067.

Bennai, R., Fourn, H., Nebab, M., Atmane, R.A., Mellal, F., Atmane, H.A., Benadouda, M. and Tounsi, A. (2022b), "On the wave dispersion and vibration characteristics of FG plates resting on elastic Kerr foundations via HSDT", *Adv. Concrete Constr.*, **14**(3), 169-183. https://doi.org/10.12989/acc.2022.14.3.169.

Bennai, R., Mellal, F., Nebab, M., Fourn, H., Benadouda, M., Atmane, H.A., Tounsi, A. and Hussain, M. (2022c), "On wave dispersion properties of functionally graded plates resting on elastic foundations using quasi-3D and 2D HSDT", *Earthq. Struct.*, **22**(5), 447-460. https://doi.org/10.12989/scs.2022.45.1.067.

Bourouis, M.E., Dahmane, M., Nebab, M., Benadouda, M., Atmane, H.A. and Bennai, R. (2025), "Elastic wave propagation and dynamic response of multidirectional FG beams under varying thermal conditions", *Mech. Bas. Des. Struct. Mach.*, **53**(12), 8086-8110. https://doi.org/10.1080/15397734.2025.2505969.

Cheng, Y.H. and She, G.L. (2025a), "Nonlinear dynamics of rotating graphene-reinforced composite blades under 1:2 internal resonance in fluid-submerged environments", *Ocean Eng.*, **341**(4), 122717. https://doi.org/10.1016/j.oceaneng.2025.122717.

Cheng, Y.H. and She, G.L. (2025b), "Nonlinear transient response of rotating graphene-reinforced metal foam beams with cracks", *Int. J. Struct. Stab. Dyn.*, 2640003. https://doi.org/10.1142/S0219455426400031.

Cheng, Y.H., She, G.L. and Eltaher, M.A. (2025), "Nonlinear internal resonance of graphene-reinforced metal foam plates with initial geometric imperfection under non-uniform temperature field", *Aerosp. Sci. Technol.*, **165**, 110491. https://doi.org/10.1016/j.ast.2025.110491.

Dahmane, M., Benadouda, M., Bensaid, I., Saimi, A. and Atmane, H.A. (2024b), "Effect of crack on the dynamic response of bidirectional porous functionally graded beams on an elastic foundation based on finite element method", *Acta Mechanica*, **235**(6), 3849-3860. https://doi.org/10.1007/s00707-024-03906-1.

Dahmane, M., Benadouda, M., Fellah, A., Saimi, A., Hassen, A.A. and Bensaid, I. (2024a), "Porosities-dependent wave propagation in bi-directional functionally graded cantilever beam with higher-order shear model", *Mech. Adv. Mater. Struct.*, **31**(26), 8018-8028. https://doi.org/10.1080/15376494.2023.2253546.

Dahmane, M., Noureddine, L., Benosman, A.S., Bennai, R., Atmane, H.A. and Benadouda, M. (2024c), "Inclined crack identification in bidirectional FG beams on an elastic foundation using the h-version of the finite element method", *Mech. Adv. Mater. Struct.*, **31**(28), 10477-10483. https://doi.org/10.1080/15376494.2023.2290226.

Debbaghi, S., Dahmane, M., Benadouda, M., Atmane, H.A., Bendenia, N. and Hadji, L. (2024), "Wave propagation of bi-directional porous FG beams using Touratier's higher-order shear deformation beam theory", *Couple. Syst. Mech.*, **13**(1), 43-60. https://doi.org/10.12989/csm.2024.13.1.043.

Djebbour, K.D., Mokhtar, N., Hassen, A.A., Alghanmi, R.A., Hadji, L. and Riadh, B. (2024), "An enhanced quasi-3D HSDT for free vibration analysis of porous FG-CNT beams on a new concept of orthotropic VE-foundations", *Mech. Adv. Mater. Struct.*, **32**(5), 893-909. https://doi.org/10.1080/15376494.2024.2356728.

Ebrahimi, F., Ghazali, M. and Dabbagh, A. (2022), "Hygro-thermo-viscoelastic wave propagation analysis of FGM nanoshells via nonlocal strain gradient fractional time-space theory", *Wave. Random Complex Media*, **35**(5), 9437-9456. https://doi.org/10.1080/17455030.2022.2105978.

Ebrahimi, F., Ghazali, M. and Dabbagh, A. (2024), "Effect of temporal nonlocality on wave propagation behaviors of viscoelastic FGM nanoshells", *J. Brazil. Soc. Mech. Sci. Eng.*, **46**(3), 126. https://doi.org/10.1007/s40430-024-04701-8.

Faleh, N.M., Ahmed, R.A. and Fenjan, R.M. (2018), "On vibrations of porous FG nanoshells", *Int. J. Eng. Sci*., **133**, 1-14. https://doi.org/10.1016/j.ijengsci.2018.08.007.

Fan, Y.H. and She, G.L. (2025), "Nonlinear transient response of axially moving graphene platelets reinforced metal foams plate with initial geometrical imperfection", *Comput. Concrete*, **36**(5), 523-531. https://doi.org/10.12989/cac.2025.36.5.523.

Fan, Y.H. and She, G.L. (2026), "Low-velocity impact response of rotating 2D-FGM annular plates with variable thickness", *Commun. Nonlin. Sci. Numer. Simul.*, **152**(Part D), 109373. https://doi.org/10.1016/j.cnsns.2025.109373.

Fan, Y.H., She, G.L. and Eltaher, M. A (2025), "Nonlinear vibrations of two-directional functionally graded spinning annular plates with variable thickness", *Thin Wall. Struct*., **216**(A), 113627. https://doi.org/10.1016/j.tws.2025.113627.

Ghalem, M., Zahaf, S., Dahmane, M., Atmane, H.A. and Bennai, R. (2025), "Natural frequencies of 2D-FG beams with internal crack defects on Winkler-Pasternak elastic foundation using finite element technique", *Mech. Bas. Des. Struct. Mach.*, **53**(7), 4948-4965. https://doi.org/10.1080/15397734.2025.2458097.

Hu, Y.D. and Li, W.Q. (2018), "Study on primary resonance and bifurcation of a conductive circular plate rotating in air-magnetic fields", *Nonlin. Dyn.*, **93**(2), 671-687. https://doi.org/10.1007/s11071-018-4217-y.

Hu, Y.D. and Li, W.Q. (2019), "Magnetoelastic axisymmetric multi-modal resonance and Hopf bifurcation of a rotating circular plate under aerodynamic load", *Nonlin. Dyn.*, **97**(2), 1295-1311. https://doi.org/10.1007/s11071-019-05049-8.

Hu, Y.D. and Ma, B.B. (2019), "Magnetoelastic combined resonance and stability analysis of a ferromagnetic circular plate in alternating magnetic field", *Appl. Math. Mech.*, **40**(7), 925-942. https://doi.org/10.1007/s10483-019-2496-7.

Hu, Y.D. and Wang, T. (2015), "Nonlinear resonance of the rotating circular plate under static loads in magnetic field", *Chin. J. Mech. Eng.*, **28**(6), 1277-1284. https://doi.org/10.3901/CJME.2015.0720.097.

Hu, Y.D. and Wang, T. (2016), "Nonlinear free vibration of a rotating circular plate under the static load in magnetic field", *Nonlin. Dyn.*, **85**(3), 1825-1835. https://doi.org/10.1007/s11071-016-2798-x.

Hu, Y.D. and Xu, H.R. (2021), "Nonlinear natural vibration of a circular plate in the non-uniform induced magnetic field", *Arch. Appl. Mech.*, **91**(6), 2513-2533. https://doi.org/10.1007/s00419-021-01901-9.

Hu, Y.D., Li, Z., Du, G.J. and Wang, Y.N. (2018), "Magneto-elastic combination resonance of rotating circular plate with varying speed under alternating load", *Int. J. Struct. Stab. Dyn.*, **18**(3), 1850032. https://doi.org/10.1142/S0219455418500323.

Jiammeepreecha, W., Chaidachatorn, K., Phungpaingam, B., Klaycham, K. and Chucheepsakul, S. (2025), "Effective nonlocal finite element formulation for free vibration analysis of S-FGM doubly curved nanoshells based on linear strain-displacement relations using TSDT", *Comput. Math. Appl.*, **179**, 77-102. https://doi.org/10.1016/j.camwa.2024.11.021.

Karami, B., Janghorban, M. and Li, L. (2018), "On guided wave propagation in fully clamped porous functionally graded nanoplates", *Acta Astronaut*., **143**, 380-390. https://doi.org/10.1016/j.actaastro.2017.12.011.

Karami, B., Shahsavari, D., Janghorban, M., Dimitri, R. and Tornabene, F. (2019), "Wave propagation of porous nanoshells", *Nanomater.*, **9**(1), 22. https://doi.org/10.3390/nano9010022.

Khaniki, H.B. and Ghayesh, M.H. (2023), "Highly nonlinear hyperelastic shells: Statics and dynamics", *Int. J. Eng. Sci.*, **183**, 103794. https://doi.org/10.1016/j.ijengsci.2022.103794.

Khayra, D., Meziane, M.A.A., Hadji, L., Atmane, H.A., Bennai, R. and Madan, R. (2024), "Effect of porosity and boundary conditions on dynamic characteristics of cracked plates made of functionally graded materials", *Adv. Concrete Constr.*, **18**(3), 175-190. https://doi.org/10.12989/acc.2024.18.3.175.

Khorshidi, S., Chakouvari, S., Askari, H. and Cveticanin, L. (2022), "Free vibrations of flexoelectric FGM conical nanoshells with piezoelectric layers: Modeling and analysis", *Energi.*, **15**(9), 2973. https://doi.org/10.3390/en15092973.

Lata, P. and Kaur, H. (2024), "Stoneley wave propagation in transversely isotropic thermoelastic media using new modified couple stress theory and two-temperature theory", *Couple. Syst. Mech.*, **13**(5), 395-409. https://doi.org/10.12989/csm.2024.13.5.395.

Li, L., Wang, J.X., Li, Z. and Huang, J.Q. (2025), "The effects of porosity on the vibration behaviors of the functionally graded spherical nanoshells using general higher-order shear deformation theory", *Mech. Solid.*, 1-16. https://doi.org/10.1134/S0025654425601776.

Li, W.Q. and Hu, Y.D. (2021), "Magneto-aeroelastic internal resonances of a rotating circular plate based on gyroscopic systems decoupling", *Int. J. Struct. Stab. Dyn.*, **21**(1), 2150010. https://doi.org/10.1142/S0219455421500103.

Li, W.Q., Hu, Y.D. and Li, Z. (2024), "Magneto-aero-elastic superharmonic and subharmonic resonances, bifurcations and chaos of conductive spinning circular plates", *Int. J. Bifurcat. Chaos*, **33**(01), 2330001. https://doi.org/10.1142/S021812742330001X.

Li, Z., Hu, Y.D. and Li, J. (2017), "Magnetoelastic principal parametric resonance of a rotating electroconductive circular plate", *Shock Vib.*, **2017**, 5196847. https://doi.org/10.1155/2017/5196847.

Ma, L.H., Ke, L.L., Reddy, J.N., Yang, J., Kitipornchai, S. and Wang, Y.S. (2018), "Wave propagation characteristics in magneto-electro-elastic nanoshells using nonlocal strain gradient theory", *Compos. Struct.*, **199**, 10-23. https://doi.org/10.1016/j.compstruct.2018.05.061.

Ma, Z.S., She, G.L. and Eltaher, M.A. (2026), "Nonlinear internal resonance in graphene platelet-reinforced metal foam plates: Straight-side quadrilateral geometry effects", *Thin Wall. Struct.*, **219**(A), 114186. https://doi.org/10.1016/j.tws.2025.114186.

Ma, Z.S., She, G.L. and Li, C. (2025), "Nonlinear thermal flutter analysis of graphene platelets reinforced metal foam arbitrary quadrilateral plates", *Arch. Civil Mech. Eng.*, **25**(4), 203. https://doi.org/10.1007/s43452-025-01262-y.

Mansouri, M., Dardel, M. and Ghasemi, M.H. (2024), "Nonlinear vibration of truncated open conical nanoshells under harmonic excitation", *Int. J. Struct. Stab. Dyn.*, **24**(22), 2450255. https://doi.org/10.1142/S0219455424502559.

Mellal, F., Bennai, R., Avcar, M., Nebab, M. and Atmane, H.A. (2023), "On the vibration and buckling behaviors of porous FG beams resting on variable elastic foundation utilizing higher-order shear deformation theory", *Acta Mechanica*, **234**(9), 3955-3977. https://doi.org/10.1007/s00707-023-03603-5.

Mellal, F., Bennai, R., Nebab, M., Atmane, H.A., Bourada, F., Hussain, M. and Tounsi, A. (2021), "Investigation on the effect of porosity on wave propagation in FGM plates resting on elastic foundations via a quasi-3D HSDT", *Wave. Random Complex Media*, **34**(5), 3727-3753. https://doi.org/10.1080/17455030.2021.1983235.

Mirfatah, S.M., Salehipour, H. and Civalek, O. (2025), "On the nonlinear forced vibration of nanoshells via nonlocal strain gradient theory", *Int. J. Eng. Sci.*, **211**, 104257. https://doi.org/10.1016/j.ijengsci.2025.104257.

Nebab, M., Atmane, H.A. and Bennai, R. (2024a), "Investigating wave propagation in sigmoid-FGM imperfect plates with accurate Quasi-3D HSDTs", *Steel Compos. Struct.*, **51**(32), 185-202. https://doi.org/10.12989/scs.2024.51.2.185.

Nebab, M., Atmane, H.A., Bennai, R. and Dahmane, M. (2024b), "Warping and porosity effects on the mechanical response of FG-Beams on non foundations via a Quasi-3D HSDT", *Struct. Eng. Mech.*, **90**(1), 83-96. https://doi.org/10.12989/sem.2024.90.1.083.

Nebab, M., Dahmane, M., Belqassim, A., Atmane, H.A., Bernard, F., Benadouda, M., Bennai, R. and Hadji,

L. (2024c), "Fundamental frequencies of cracked FGM beams with influence of porosity and Winkler/Pasternak/Kerr foundation support using a new quasi-3D HSDT", *Mech. Adv. Mater. Struct.*, **31**(28), 10639-10651. https://doi.org/10.1080/15376494.2023.2294371.

She, G.L. and He, Y.J. (2025), "Nonlinear 1:1 internal resonance in graphene platelet-reinforced fluid-conveying pipes", *Appl. Math. Mech.*, **46**(10), 1903-1920. https://doi.org/10.1007/s10483-025-3305-8.

She, G.L., Ren, Y.J. and Li, A. (2026), "Nonlinear low-velocity impact on axially-functionally-graded graphene-platelet-reinforced metal-foam cylindrical shells", *Struct. Eng. Mech.*, **97**(1), 89-105. https://doi.org/10.12989/sem.2026.97.1.089.

Thuy, T.T.T., Tu, N.A., Thien, N.A. and Thanh, N.T. (2025), "Random vibration of two-curvature nanoshells with piezoelectric layers resting on viscoelastic foundations", *Thin Wall. Struct.*, **209**, 112948. https://doi.org/10.1016/j.tws.2025.112948.

Van, K., Van, M.P. and Duc, N.D. (2025), "Free and forced vibration analysis of tri-directional functionally graded porous doubly-curved nanoshells integrated with magneto-electro-elastic layers", *Comput. Struct.*, **318**, 107964. https://doi.org/10.1016/j.compstruc.2025.107964.

Van, P.V., Tounsi, A. and Belarbi, M.O. (2023), "On the nonlocal free vibration analysis of functionally graded porous doubly curved shallow nanoshells with variable nonlocal parameters", *Eng. Comput.*, **39**(1), 835-855. https://doi.org/10.1007/s00366-022-01687-6.

Vinh, P.V. and Tounsi, A. (2022), "Free vibration analysis of functionally graded doubly curved nanoshells using nonlocal first-order shear deformation theory with variable nonlocal parameters", *Thin Wall. Struct.*, **174**, 109084. https://doi.org/10.1016/j.tws.2022.109084.

Wang, X.T., Liu, J., Hu, B., Li, Z.N. and Zhang, B. (2023b), "Wave propagation in porous functionally graded piezoelectric nanoshells resting on a viscoelastic foundation", *Physica E: Low Dimens. Syst. Nanostruct.*, **151**, 115615. https://doi.org/10.1016/j.physe.2022.115615.

Wang, X.T., Liu, J., Hu, B., Zhang, B. and Shen, H.M. (2023a), "Wave propagation responses of porous bi-directional functionally graded magneto-electro-elastic nanoshells via nonlocal strain gradient theory", *Appl. Math. Mech.*, **44**(10), 1821-1840. https://doi.org/10.1007/s10483-023-3043-7.

Wang, Y.Q., Liang, C. and Zu, J.W. (2019), "Wave propagation in functionally graded cylindrical nanoshells based on nonlocal Flugge shell theory", *Eur. Phys. J. Plus*, **134**(5), 233. https://doi.org/10.1140/epjp/i2019-12543-0.

Zeighampour, H., Beni, Y.N. and Karimipour, I. (2017), "Material length scale and nonlocal effects on the wave propagation of composite laminated cylindrical micro/nanoshells", *Eur. Phys. J. Plus*, **132**(12), 503. https://doi.org/10.1140/epjp/i2017-11770-7.

Zhao, B. and She, G.L. (2025), "Vibration analysis of graphene reinforced metal foam coupled plates under arbitrary boundary and coupled conditions", *Eng. Struct.*, **343**(C), 121143. https://doi.org/10.1016/j.engstruct.2025.121143.

Zhao, B., Eltaher, M.A. and She, G.L. (2025), "Dynamic response analysis of acoustic black hole plates with cutouts under arbitrary boundary constraints", *Thin Wall. Struct.*, **217**(Part A), 113859. https://doi.org/10.1016/j.tws.2025.113859.